View metadata, citation and similar papers at core.ac.uk

brought to you by CORE

provided by University of Liverpool Repository

Multidisciplinary | Rapid Review | Open Access Journal

Date of publication xxxx 00, 0000, date of current version xxxx 00, 0000.
Digital Object Identifier 10.1109/ACCESS.2018.Doi Number

Lightweight and Low-loss 3-D Printed Millimeter-Wave Bandpass Filter Based on Gap-Waveguide

BAHAA AL-JUBOORI[1,2], JIAFENG ZHOU[1], YI HUANG[1], (Senior Member, IEEE), MUAAD HUSSEIN[1], AHMED ALIELDIN[1], (Member, IEEE), WILLIAM J. OTTER[3], DIRK KLUGMANN[4], (Member, IEEE), AND STEPAN LUCYSZYN[3], (Fellow, IEEE)

[1]Department of Electrical Engineering and Electronics, University of Liverpool, Liverpool, L69 3GJ, U.K.
[2]Department of Electronic and Communications Engineering, Al-Nahrain University, Baghdad, 10070, Iraq.
[3]Department of Electrical and Electronic Engineering, Imperial College London, London, SW7 2AZ, U.K.
[4]S&AO Ltd and UKRI / STFC Rutherford Appleton Laboratory, Harwell Campus, Didcot, OX11 0QX, U.K.

Corresponding author: Jiafeng Zhou (e-mail: Jiafeng.Zhou@liverpool.ac.uk).

This work was supported by the Industrial Strategy Challenge Pump Priming Fund, U.K., and the Higher Committee for Education Development (HCED), Iraq, under Sponsorship D-10/66, and the UK Space Agency grant entitled '3D printed millimetre-wave components for guided-wave and quasi-optical systems for spacecraft payloads' NSTP3-FT-046.

ABSTRACT This paper presents a comprehensive study of a groove gap waveguide (also known as a waffle-iron) bandpass filter at Ka-band (26.5-40 GHz), fabricated using high resolution polymer jetting (Polyjet) 3-D printing technology. The same filter was previously fabricated using brass CNC milling technology. The metalized Polyjet 3-D printed filter is lower loss, lighter in weight and more cost-effective, when compared to the solid metal case. The filter operates at a center frequency of 35.65 GHz and has a 500 MHz bandwidth (1.4% fractional bandwidth), having a transmission zero below and above the passband. Without any design iterations, the measured S-parameters for the Polyjet 3-D printed filter are presented and compared with simulated results, showing excellent agreement. A comparison is then made between the measured results and that of its brass machined counterpart. The new Polyjet 3-D printed filter is 85% lighter than the conventional machined version. All these features prove the important potential of 3-D printing technology for millimeter-wave applications, which include aerospace.

INDEX TERMS 3-D printing, bandpass filter, millimeter-wave band, gap waveguide, waffle-iron, Polyjet.

I. INTRODUCTION

Low loss, low mass and easy of manufacture for bandpass filters (BPFs) operating at millimeter-wave (mm-wave) frequencies are of high importance for aerospace (unmanned drone, manned aircraft, satellite and interplanetary mission) applications. A large number of mm-wave BPFs using various design and fabrication technologies have been reported over the past few decades. For high frequency microwave/mm-wave applications, designers prefer metal-pipe rectangular waveguide solutions, due to their low loss and high power handling capabilities. Typical examples of waveguide BPF implementations have been demonstrated at X-band (8.2-12.4 GHz) [1] and Ku-band (12.4-18 GHz) [2]. One of the drawbacks with conventional waveguide components is the poor electrical contact between joined waveguide parts, especially at mm-wave frequencies. To mitigate this, very accurate machining is required, which results in higher costs. In contrast, planar solutions are compatible with monolithic microwave integrated circuit (MMIC) applications, although the associated ohmic losses are relatively high, especially at mm-wave frequencies [3][4]. Substrate integrated waveguide (SIW) technology has also been used to implement BPFs at mm-wave frequencies [5]. Although SIWs present good integration capabilities, when compared to conventional waveguides, they can still suffer from high dielectric losses. Air-filled SIW [6] and empty SIW (ESIW) [7][8] have been proposed for manufacturing empty waveguides without having a dielectric substrate, but at the same time completely integrated into a planar substrate. This method is a compromise between the advantages of classical waveguide technologies, such as high quality (Q-)factor and low losses, and the advantages of planar circuits, such as low cost and easy compact integration. However, the Q-factor is still much lower than the conventional rectangular waveguides. This is because the conventional waveguides are much higher, which means more volume and more energy can be stored than in ESIWs (having the same height of the

dielectric substrate in SIW). To overcome this restriction, a novel integrated structure was proposed [9] to embed very high Q-factor filters based on the ESIW with an increased height. Nonetheless, due to the use of microstrip feed lines and transitions (from microstrip to ESIW), losses will increase.

Gap waveguide was proposed as an alternative to conventional metal-pipe rectangular waveguides, at extremely high frequencies (EHF) and beyond [10], as it avoids the use of (relatively lossy – e.g. typically 6 dB m^{-1} at W-band) sidewalls. Due to the small dimensions of the structures at mm-wave frequencies, fabrication of conventional waveguide components using longitude-cut fabrication techniques is challenging, due to radiation leakage from the physical connection mismatches of the waveguide pieces. Moreover, poor metal contact also leads to other undesirable effects, such as passive intermodulation (PIM). Gap waveguides consist of two parallel plates, being open from the sides. One of the plates is flat, which ideally acts as a perfect electrical conducting plane, while the other has a periodic structure of metal pins that are created to act as an artificial magnetic conductor [10][11]. By choosing specific pin dimensions, a cut-off frequency for parallel-plate modes can be established; prohibiting wave propagation. To provide a path for electromagnetic propagation, a groove gap waveguide (GGW) or ridge gap waveguide is formed among the pins, where the waves transfer over the resonators through the groove or ridge, respectively [10][12]. Similar to conventional rectangular waveguides, gap waveguides are usually manufactured using machining technology (e.g., by milling or drilling metal structures).

Low-cost gap waveguides have been proposed [13]-[16]. In the former two, half-height pins are employed in gap waveguide technology, making fabrication processing of the pin surface easier. However, an accurate manufacturing process is still needed. In the latter two, a novel cost-effective method to manufacture integrated waveguide structures at high frequencies has been presented. In this method, instead of pins, a truncated glide-symmetric holey EBG structure is adopted.

Gap waveguides are regarded as a compromise solution for mm-wave BPFs. Unlike planar and SIW technologies, gap waveguide filters are characterized by their high Q-factor and, thus, low losses at mm-wave frequencies. Also, the relatively lossy sidewalls between the top and bottom plates (found with conventional waveguides) are no longer needed, where periodic pins can be created on the borders of one of the parallel plates (in order to function as a high impedance surface). Over the last few years, many BPFs have been reported based on gap waveguide (also known as waffle-iron) technology at X-band [17][18], Ku-band [12], Ka-band (26.5-40 GHz) [19]-[21], Q-band (33-50 GHz) [22] and V-band (50-75 GHz) [23].

In this work, a low loss, lightweight and easy to manufacture GGW BPF was fabricated using, for the first time, high resolution Polyjet 3-D printing. This paper is organized as follows: Section II introduces a study of the main manufacturing techniques used to fabricate mm-wave filters. A BPF design procedure is shown in Section III. Simulation, fabrication and measurements for a prototype are described in Section IV, with a conclusion in Section V.

II. MILLIMETER-WAVE FILTER FABRICATION

Manufacturing microwave components to higher levels of accuracy, than those found at longer wavelengths, becomes increasingly more difficult as frequency increases. Different technologies can be adopted for the manufacture of BPFs operating at mm-wave frequencies. The choice of a manufacturing technology, to some extent, depends on the technology on which the filter is designed. For example, with conventional filter designs based on planar technology, printed circuit board (PCB) [24] or micromachining technology is adopted for manufacturing; while machining technology is used to fabricate waveguide or gap waveguide based filters. The merits and challenges of the four main manufacturing technologies that can be utilized to fabricate mm-wave BPFs will be briefly discussed.

A. CO-FIRED CERAMIC

For harsh environments, including high humidity and high-temperatures, co-fired ceramic technology can be a good choice for component fabrication. Low temperature co-fired ceramic (LTCC) technology, with sintering below 1,000°C, is used to produce compact multilayer circuits. LTCC has been used to implement different mm-wave BPFs; for example, planar-based filter of 60 GHz [25][26] and SIW-based filter at 40 GHz [5], 140 GHz [27][28] and 174 GHz [29]. LTCC technology has many advantages for the manufacture of microwave BPFs. For example, ceramic materials provide highly robust performance under stringent environmental and mechanical conditions. Furthermore, unlike micromachining, 3-D structures having complex designs can be realized with a cost-effective fabrication technique, especially for medium and high volumes of manufacture. Having said this, LTCC-based mm-wave BPFs suffer from notably high insertion loss, when compared to some other fabrication technologies, such as machining and 3-D printing. Therefore, it is not desirable for the fabrication of high Q-factor and low-loss components.

B. MICROMACHINING

Both bulk or surface micromachining technologies can be used to implement BPFs at (sub-)mm-wave frequencies [30]. Two waveguide filters, one operating in the WR-3 band (220-325 GHz) and the other in the WR-1.5 band (500-750 GHz), were fabricated using SU-8. A comparative manufacturing study of sub-THz bandpass frequency selective surface (FSS) filters has been reported [31]. Photolithography facilitates batch processing, when compared to the other methods. However, the need for cleanroom microfabrication processing increases complexity, time to manufacture and ultimately cost.

C. MACHINING

Machining technology is mainly used for metal-based component fabrication. For high Q-factor and low-loss BPFs, air-filled metal-pipe rectangular waveguide or gap waveguide technologies can be adopted. In recent years, many waveguide- and gap waveguide-based mm-wave BPFs have been fabricated using machining technology, by milling out or drilling into metal structures [2], [19]-[21], [32] and [33]. Machining technology is preferred for high-Q and low-loss components within the mm-wave band. However, the small dimensions of their structures (e.g., pin arrays in gap waveguide) increase the complexity of the milling or drilling process in machining technology and, hence, also the time and cost of fabrication. Additionally, with aerospace and satellite applications, excess mass is also an important factor.

D. 3-D PRINTING

3-D printing technology is emerging for the fabrication of lightweight and low-loss components, as well as complex structured components operating at mm-wave frequencies [34]-[37]. 3-D printing technology can be mainly classified as either metal-based or polymer-based (with additional metal plating) 3-D printing. With the former, binder jetting/sintering and selective laser melting (SLM) can be adopted to construct metal-pipe rectangular waveguides, with Cu-15Sn powder melted layer by layer [38]. With the latter, metal-pipe rectangular waveguides have been demonstrated using fused deposition modelling (FDM) [36], stereolithographic apparatus (SLA) [36] and polymer-jetting (Polyjet) [39]. A variety of GGW-based prototypes operating at the Ka-band and manufactured by metallized 3-D printing technique have been presented [40]. Their work proved the potential of using 3-D printing technology to fabricate GGW structures at high frequencies. Furthermore, 3-D printing and metallization technology is adopted to fabricate a novel leaky-wave antenna based on gap waveguide technology [41]. In the work reported here, Polyjet 3-D printing of a groove gap waveguide BPF is demonstrated for the first time.

III. FILTER DESIGN

A. FILTER SPECIFICATIONS AND SYNTHESIS

To verify the proposed 3-D printing techniques, a mm-wave BPF is designed and fabricated, having the high selectivity design specifications given in TABLE I. In this work, a high selectivity response is achieved with a lower number of resonators by introducing cross-coupling between one pair of non-adjacent resonators, to produce two transmission zeros around the passband. The resulting topology of this compact BPF is shown in FIGURE 1. The coupling coefficient (M) between resonators and external quality factor (Q_e) can be determined from the circuit elements of the low-pass prototype filter [42]. With reference to FIGURE 1, M_{ij} is the coupling coefficient between two resonators, where i and j identify different resonator numbers. These values are: M_{12} = M_{34} = 0.0168, M_{23} = 0.0154, M_{14} = -0.0043 and Q_e = 48.878.

TABLE I
TARGET BAND-PASS FILTER DESIGN SPECIFICATIONS

Parameter	Value
Filter Type	Quasi-elliptic
Center Frequency (GHz)	35.65
Fractional Bandwidth (*FBW*) (%)	1.4
Insertion Loss (dB)	< 0.5
Return Loss (dB)	> 15

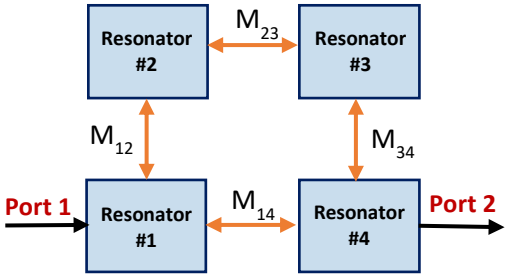

FIGURE 1. Topology of the filter.

B. DESIGN CURVES

On the (bottom) plate containing the periodic array of pins, the tips of these pins are separated from the (top) flat plate with a gap (g). Based on the dispersion diagram [43], the dimensions of the unit cell are chosen to cover Ka-band, as shown in FIGURE 2. In gap waveguide, the height of the pins $h \sim \lambda_o/4$ and the air gap separation distance $g < \lambda_o/4$, where λ_o is the wavelength in free space. To create a groove gap waveguide, some of the pins are removed to form four air-filled cavity resonators (named grooves), as illustrated in FIGURE 2. To obtain a resonance at 35.65 GHz, initially, the geometric shape of the cavities was chosen to be cubic. The length and width of each cavity is approximately a half guide-wavelength at the desired midband frequency (f_o), $\lambda_g/2$, while the height is chosen to be equal to the height of a rectangular waveguide WR28, i.e. the shorter dimension of the rectangular waveguide. The associated cavity mode is confined between the flat areas of both parallel plates and rows of side pins. Increasing the number of side pins rows, decreases the undesired leakage. However, it increases the structure complexity. In this work, to reduce the complexity of the structure with a reasonable leakage, two rows of side pins are sufficient. FIGURE 3(a) and (b) exhibit the electric field for a single gap waveguide resonator with two and three rows of side pins, respectively. It can be noticed that the leakage at the third row of sided pins in FIGURE 3(b) is lower than -40 dB which can be neglected. The resonance frequency of each resonator can be determined from its dimensions. With our design, the 35.65 GHz cavity resonator was achieved with spatial dimensions of 5.9×5.9×3.1 mm^3. To achieve cross-resonator coupling, a coupling pillar (P_{mn}) is longitudinally centered in parallel with two periodic pins between any two adjacent resonators, as illustrated in FIGURE 4.

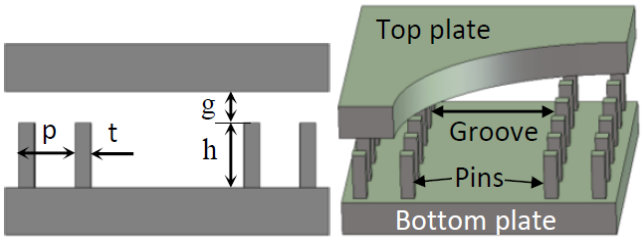

FIGURE 2. Gap waveguide periodic structure: (a) Cross-section; (b) 3D perspective view. (Dimensions listed in TABLE II).

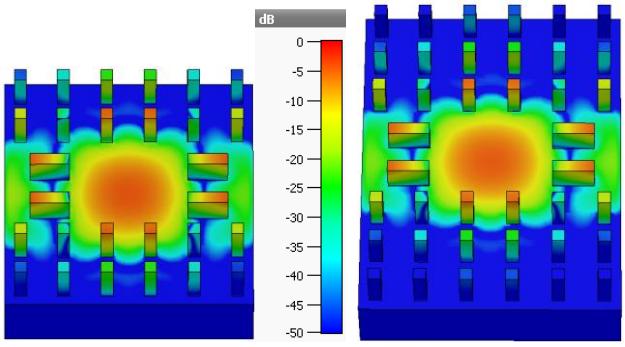

FIGURE 3. Electric field pattern of one resonator in groove gap waveguide with side pins. (a)Two rows. (b) Three rows.

To study the effect of each spatial dimension, the normalized coupling coefficient between Resonators #1 and #2, m_{12} ($m_{12} = M_{12} / FBW$), is plotted as a function of the pillar length (P_{12_l}) and pillar height (P_{12_h}), as illustrated in FIGURE 5. These plots are the design curves for the normalized coupling coefficient m between adjacent resonators. Due to symmetry, P_{12} and P_{34} are identical. The dimensions of P_{23} were evaluated in the same way (results not shown). To achieve cross-resonator coupling, a pair of inductive irises are placed between Resonators #1 and #4, as illustrated in FIGURE 4. The thickness of these irises is the same as the pins, and their height ($iris\_h$) is fixed to pin height plus gap separation distance (i.e., the irises touch the internal surfaces of both plates). The normalized coupling coefficient m_{14} is plotted as a function of the iris width ($iris\_w$), as shown in FIGURE 5.

TABLE II
INITIAL AND OPTIMIZED BPF SPATIAL DIMENSIONS (mm)

Parameter	Description	Initial Value	Optimized Value
g	gap separation	1.00	1.00
t	pin thickness	0.50	0.70
h	pin height	2.00	2.10
p	pin period	2.00	2.20
P_{12_h}	pillar height for Res. #1_Res. #2	1.72	1.70
P_{12_l}	pillar length for Res. #1_Res.# 2	1.27	1.25
P_{23_h}	pillar height for Res. #2_Res. #3	2.20	2.33
P_{23_l}	pillar length for Res. #2 _Res. #3	1.50	1.70
$iris\_h$	iris height	3.00	3.10
$iris\_w$	iris width	1.92	1.90
H_h	input/output pillar height	1.64	1.67
H_l	input/output pillar length	0.91	0.92

Couplings between the input source and Resonator #1 and also between Resonator #4 and the output load, are realized by placing two pairs of pillars (H), with the first and fourth resonators connected to WR-28 rectangular waveguide ports, respectively. The length of H (H_l) controls the resonance frequency, while its height (H_h) controls the external quality factor, as shown in FIGURE 6. Although the resonance frequency is slightly affected by changes of input/output pillar height, this can be compensated by optimizing the input/output pillar length. The initial structural dimensions are given in TABLE II. A final optimization process is then applied to fine tune the spatial dimensions of the filter structure, to fully meet the target frequency response specifications.

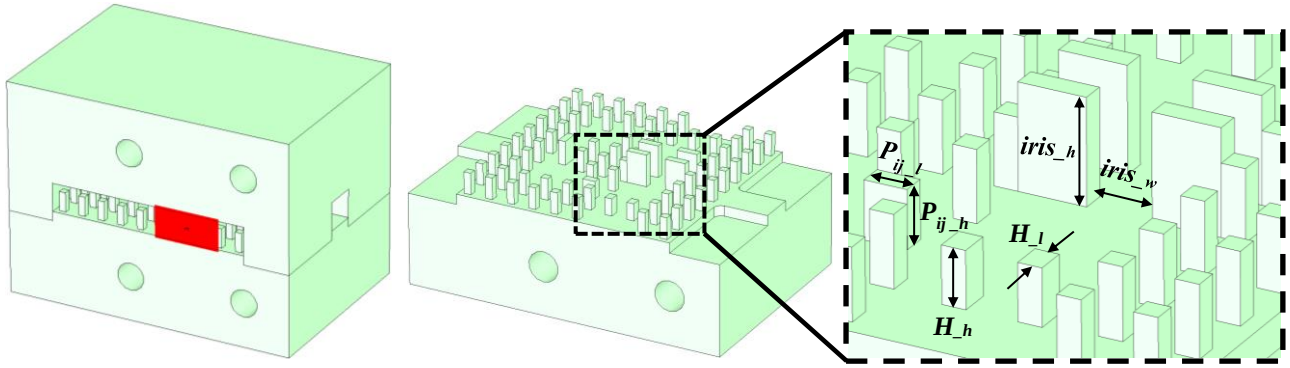

FIGURE 4.Proposed filter structure (dimensional values listed in TABLE II).

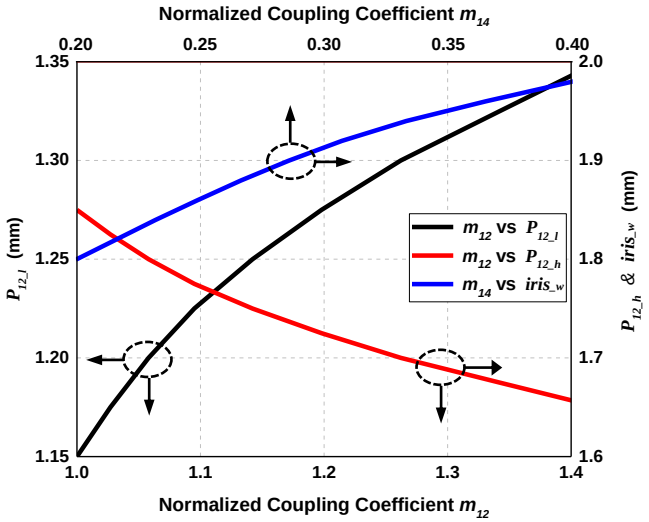

FIGURE 5. Normalized coupling coefficients m_{12} as a function of P_{12_l} and P_{12_h}, and m_{14} as a function of $iris_w$ (with $iris_h = h + g$).

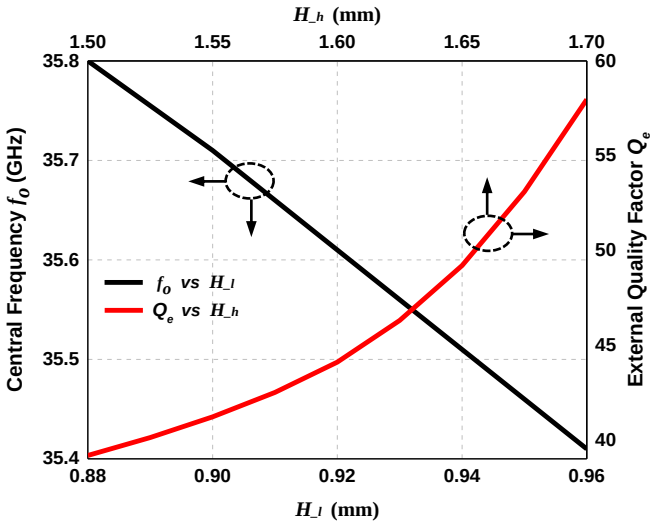

FIGURE 6. Center frequency of a doubly-loaded resonator as a function of H_l (H_h = 1.5 mm) and the external quality factor as a function of H_h (H_l = 1.2 mm).

IV. SIMULATIONS AND MEASUREMENTS

A. SIMULATED RESULTS

Full-wave electromagnetic simulations were undertaken using CST MICROWAVE STUDIO®. The metal was modeled as copper. The whole structure of the optimized BPF is shown in FIGURE 4. FIGURE 7 shows the simulated scattering (S)-parameters of the final optimized filter. It can be seen that the simulated performance satisfies the design specifications. The minimum insertion loss *IL* within the passband is 0.4 dB (with a passband average of 0.45 dB) and the passband return loss *RL* is better than 22 dB. Two transmission zeros are introduced at 34.89 GHz and 36.52 GHz, as a result of the cross-coupling between Resonators #1 and #4. Near-symmetrical bandstop attenuation of ~50 dB is predicted.

B. FABRICATION PROCESSING

As illustrated in FIGURE 4, the filter structure is split into two parts; this simplifies the fabrication process of the pins, as well as to avoid problems with metal plating. The filter was fabricated using a 3D Systems' Projet 2500 printer, which provides near state-of-the-art resolution (800 × 900 × 790 DPI, 32 µm layers). The parts are formed by jetting of photopolymers from multiple nozzles, to form each layer that are immediately selectively UV cured, to form structure and support areas as defined by the CAD file. This technology represents the highest resolution in the commercial 3-D printing of plastics that can be achieved for large structures. Once printed, the parts are baked at 60˚C, to allow the supporting wax to melt away. To further remove any wax residue, the parts are cleaned further in a 70˚C ultrasonic bath of EZ-Rinse for 15 minutes and a room temperature ultrasonic bath of IPA for 15 minutes. These cleaned parts were then commercially electroless-plated with 20 µm thick copper, exceeding five skin depths of thickness at the lowest frequency of operation. The final Polyjet 3-D printed and copper-plated BPF prototype is shown in FIGURE 8(a).

C. MEASURED RESULTS

The prototype BPF was measured using an Anritsu 37369A vector network analyzer (VNA) with standard WR-28 waveguide flange interfaces. A Thru-Reflect-Line (TRL) calibration technique was first performed to calibrate the VNA. The measured results are shown in FIGURE 7. At the center frequency, the measured insertion and return losses are 0.5 dB and 21 dB, respectively; only 0.1 dB and 1 dB different from predictions, respectively. The measured transmission zeros are slightly further out than predicted. This is mainly due to the manufacturing tolerance. The width of the irises between Resonators #1 and #4 is a few microns shorter than in the design. Nevertheless, it should be noted that there were no iterations to the fabrication and no tuning was needed to achieve these measured results.

The measured results of the 3-D printed filter are compared with our previous design [21], as shown in FIGURE 8(b), which was fabricated from brass using a machining technology. Here, a computer numerical control (CNC) milling machine was used to create the periodic structure and four cavities on the bottom plate. The measured forward transmission and reflection coefficients, S_{21} and S_{11}, respectively, of both filters are shown in FIGURE 9, along with the simulated results. It can be seen that there are obvious differences between the measured results of the 3-D printed and machined filters. The measured insertion and return losses for the machined filter were 1.2 dB and 11 dB, respectively; significantly worse than with the new Polyjet 3-D printed counterpart. The insertion loss is more with the CNC BPF, because of the lower bulk conductivity of brass when compared to copper.

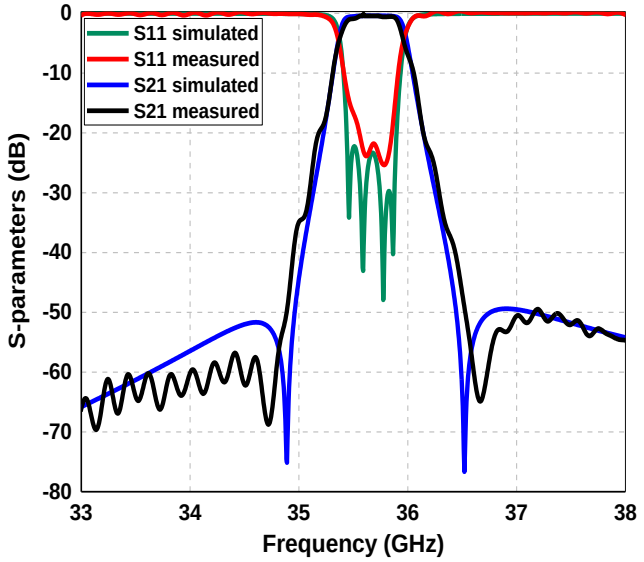

FIGURE 7. Simulated and measured results for the Polyjet 3-D printed BPF.

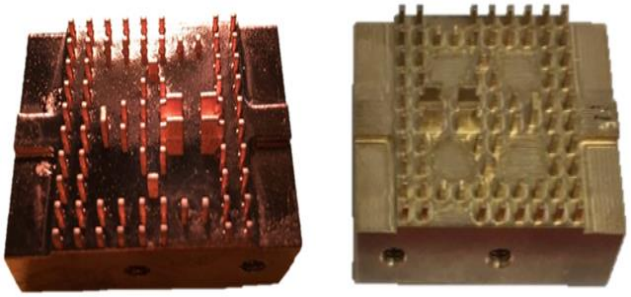

(a) (b)

FIGURE 8. Prototype Ka-band BPFs: (a) Polyjet 3-D printed (weighing 17 g); and (b) CNC machined (weighing 112 g).

Moreover, when compared to the machined filter, very little frequency shift is observed with the Polyjet 3-D printed counterpart. These improvements are mainly due to the high fabrication accuracy offered by Polyjet 3-D printing. In addition to the excellent measured performance, another important advantage of the 17 g Polyjet 3-D printed component is the dramatic reduction in mass, when compared to the 112 g brass CNC machined counterpart; an 85% weight reduction, while having the same geometric dimensions. Finally, TABLE III compares the filter with recently reported mm-wave GGW-based BPFs, fabricated using machining technology (mass was not included, due to a lack of available data). It can be seen that our Polyjet 3-D printed BPF has the lowest insertion loss and the second narrowest bandwidth.

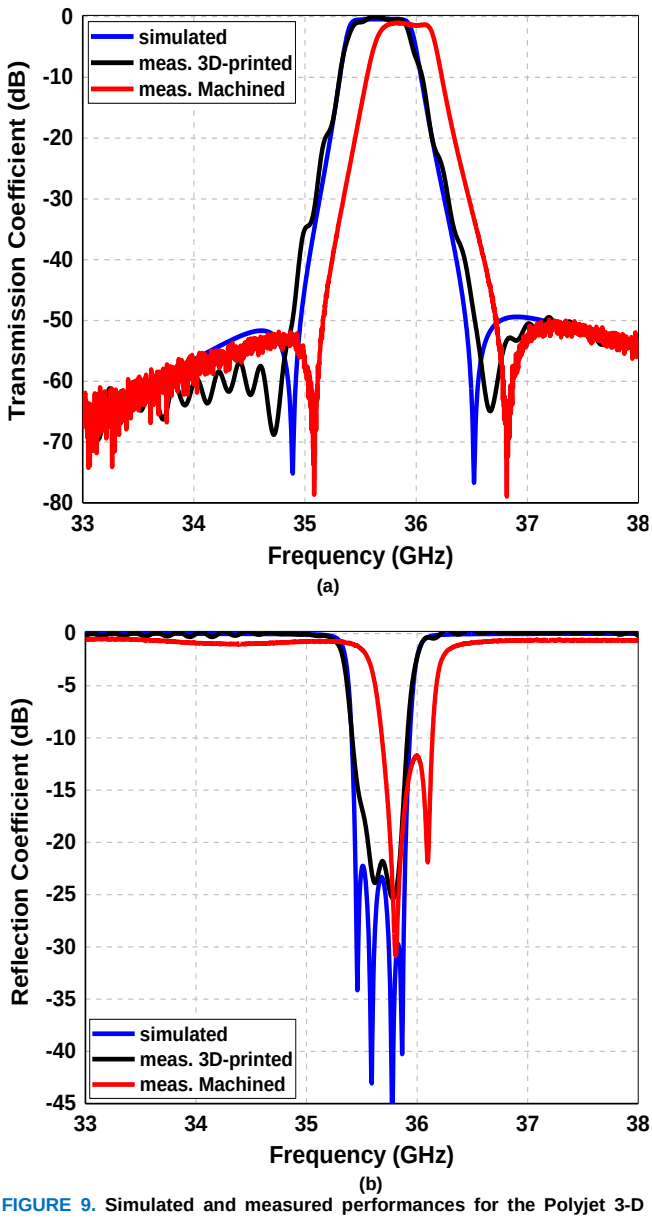

FIGURE 9. Simulated and measured performances for the Polyjet 3-D printed and machined prototype Ka-band BPFs: (a) transmission responses; (b) reflection responses.

Furthermore, good selectivity was achieved with high stopband attenuation. Clearly, the low mass and excellent measured performance of our prototype filter make it ideally suited for aerospace applications. For such applications, development time and all associated cost are also important drivers – the proposed fabrication technology has the advantages of short production development time and relatively low material costs.

TABLE III
COMPARISON OF MM-WAVE GGW-BASED BPFS FABRICATED USING IN DIFFERENT TECHNOLOGIES

Frequency (GHz)	Manufacturing Technology	Filter Order	*FBW* (%)	*IL* (dB)	*RL* (dB)	Stopband Rejection (dB)	Q_u	Dimensions (mm)	Ref.
37.37	CNC Machining	7	1.5	1	17	60	2000	61.6×12.0×2.8	[19]
35	CNC Machining	3	1	1	9	35	1091	17.8×16.0×12.7	[20]
35.65	CNC Machining	4	1.4	1.2	11.7	48	614	21.0×21.0×3.1	Previous work [21]
61	CNC Machining	5	2.5	1.5	13	60	677	-	[23]
35.65	**Polyjet 3-D Printing**	**4**	**1.4**	**0.5**	**21**	**52**	**1275**	**21.0×21.0×3.1**	**This work**

V. CONCLUSION

For the first time, Polyjet 3-D printing has been adopted to manufacture a GGW-based BPF operating at mm-wave frequencies. The 35.65 GHz 3-D printed filter presents many advantages, when compared to other manufacturing technologies, in terms of mass, performance, development time and cost. The measured results of the Polyjet 3-D printed filter are in very good agreement with predictions, without having any design iterations or post-fabrication tuning. A high selectivity has been realized by cross-coupling between two non-adjacent resonators. The locations of the transmission zeros in the measurement are slightly further away from those seen in simulations. This is mainly because of a small fabrication error; easily corrected by introducing a single design-print iteration. The Polyjet 3-D printed BPF has been compared with the same filter fabricated using a CNC milling machine. Our new BPF has a dramatically reduced mass, lower insertion loss and less frequency shift. Finally, when compared to recently reported mm-wave GGW-based BPFs, our Polyjet 3-D printed filter exhibits excellent insertion loss and frequency selectivity and has a very low mass.

REFERENCES

[1] C. Carceller, P. Soto, V. E. Boria, and M. Guglielmi, "Design of hybrid folded rectangular waveguide filters with transmission zeros below the passband," *IEEE Trans. Microw. Theory Tech.*, vol. 64, no. 2, pp. 475–485, Feb. 2016.

[2] Y.-S. He, A. Barannik, N. Cherpak, L. Sun, V. Skresanov, Y. Bian, J. Wang, M. Natarov, and V. Zolotaryov, "Novel design of band-pass waveguide filter with HTS E-plane insert," *IEEE Trans. Appl. Supercond.*, vol. 27, no. 4, pp. 4–7, Jun. 2017.

[3] I. D. Robertson and S. Lucyszyn (Editors), "RFIC and MMIC Design and Technology", Published by the IEE, Nov. 2001.

[4] S. Lucyszyn (Editor), "Advanced RF MEMS", Cambridge University Press, Cambridge, Aug. 2010.

[5] S.-W. Wong, R. S. Chen, K. Wang, Z.-N. Chen, and Q.-X. Chu, "U-shape slots structure on substrate integrated waveguide for 40-GHz bandpass filter using LTCC technology," *IEEE Trans. Components, Packag. Manuf. Technol.*, vol. 5, no. 1, pp. 128–134, Jan. 2015.

[6] F. Parment, A. Ghiotto, T. Vuong, J. Duchamp and K. Wu, "Air-filled substrate integrated waveguide for low-loss and high power-handling millimeter-wave substrate integrated circuits," in *IEEE Transactions on Microwave Theory and Techniques*, vol. 63, no. 4, pp. 1228-1238, April 2015.

[7] A. Belenguer, H. Esteban and V. E. Boria, "Novel empty substrate integrated waveguide for high-performance microwave integrated circuits," in *IEEE Transactions on Microwave Theory and Techniques*, vol. 62, no. 4, pp. 832-839, April 2014.

[8] A. L. Borja, A. Belenguer, H. Esteban and V. E. Boria, "design and performance of a high-Q narrow bandwidth bandpass filter in empty substrate integrated coaxial line at Ku-band," in *IEEE Microwave and Wireless Components Letters*, vol. 27, no. 11, pp. 977-979, Nov. 2017.

[9] J. A. Martinez, J. J. de Dios, A. Belenguer, H. Esteban and V. E. Boria, "Integration of a very high quality factor filter in empty substrate-integrated waveguide at Q-band," in *IEEE Microwave and Wireless Components Letters*, vol. 28, no. 6, pp. 503-505, June 2018.

[10] P.-S. Kildal, E. Alfonso, A. Valero-Nogueira, and E. Rajo-Iglesias, "Local metamaterial-based waveguides in gaps between parallel metal plates," *IEEE Antennas Wirel. Propag. Lett.*, vol. 8, pp. 84–87, Feb. 2009.

[11] M. G. Silveirinha, C. A. Fernandes, and J. R. Costa, "Electromagnetic characterization of textured surfaces formed by metallic pins," *IEEE Trans. Antennas Propag.*, vol. 56, no. 2, pp. 405–415, Feb. 2008.

[12] A. U. Zaman, P.-S. Kildal, and A. A. Kishk, "Narrow-band microwave filter using high-Q groove gap waveguide resonators with manufacturing flexibility and no sidewalls," *IEEE Trans. Components, Packag. Manuf. Technol.*, vol. 2, no. 11, pp. 1882–1889, Nov. 2012.

[13] F. Fan, J. Yang and P. Kildal, "Half-height pins - a new pin form in gap waveguide for easy manufacturing," *2016 10th European Conference on Antennas and Propagation (EuCAP)*, Davos, 2016, pp. 1-4.

[14] F. Fan, J. Yang, V. Vassilev and A. U. Zaman, "Bandwidth investigation on half-height pin in ridge gap waveguide," in *IEEE Transactions on Microwave Theory and Techniques*, vol. 66, no. 1, pp. 100-108, Jan. 2018.

[15] M. Ebrahimpouri, E. Rajo-Iglesias, Z. Sipus and O. Quevedo-Teruel, "Cost-effective gap waveguide technology based on glide-symmetric holey EBG structures," in *IEEE Transactions on Microwave Theory and Techniques*, vol. 66, no. 2, pp. 927-934, Feb. 2018.

[16] E. Rajo-Iglesias, M. Ebrahimpouri and O. Quevedo-Teruel, "Wideband phase shifter in groove gap waveguide technology implemented with glide-symmetric holey EBG," in *IEEE Microwave and Wireless Components Letters*, vol. 28, no. 6, pp. 476-478, June 2018.

[17] M. S. Sorkherizi, A. Khaleghi, and P.-S. Kildal, "Direct-coupled cavity filter in ridge gap waveguide," *IEEE Trans. Components, Packag. Manuf. Technol.*, vol. 4, no. 3, pp. 490–495, Mar. 2014.

[18] M. S. Sorkherizi and A. A. Kishk, "Completely tuned coupled cavity filters in defected bed of nails cavity," *IEEE Trans. Components, Packag. Manuf. Technol.*, vol. 6, no. 12, pp. 1865-1872, Dec. 2016.

[19] E. A. Alos, A. U. Zaman, and P.-S. Kildal, "Ka-band gap waveguide coupled-resonator filter for radio link diplexer application," *IEEE Trans. Components, Packag. Manuf. Technol.*, vol. 3, no. 5, pp. 870–879, Jan. 2013.

[20] B. Ahmadi and A. Banai, "Direct coupled resonator filters realized by gap waveguide technology," *IEEE Trans. Microw. Theory Tech.*, vol. 63, no. 10, pp. 3445–3452, Aug. 2015.

[21] B. Al-Juboori, Y. Huang, D. Klugmann, M. Hussein and J. Zhou, "Millimeter wave cross-coupled bandpass filter based on groove gap

waveguide technology," *UK-Europe-China Workshop on Millimetre Waves and Terahertz Technologies (UCMMT)*, Liverpool, 2017, pp. 1-4.

[22] A. del Olmo-Olmeda, M. Baquero-Escudero, V. E. Boria-Esbert, A. Valero-Nogueira and A. J. Berenguer-Verdú, "A novel band-pass filter topology for millimeter-wave applications based on the groove gap waveguide," *2013 IEEE MTT-S International Microwave Symposium Digest (MTT)*, Seattle, WA, 2013, pp. 1-4.

[23] A. Berenguer, M. Baquero-Escudero, D. Sanchez-Escuderos, B. Bernardo-Clemente and V. E. Boria-Esbert, "Low insertion loss 61 GHz narrow-band filter implemented with Groove Gap Waveguides," *European Microwave Conference*, Rome, 2014, pp. 191-194.

[24] C. E. Chrisostomidis, M. Guglielmi, P. R. Young, and S. Lucyszyn, "Application of chained functions to low-cost microwave band-pass filters using standard PCB etching techniques", *European Microwave Conference Proceedings*, Paris, France, vol. 3, pp. 40-43, Oct. 2000.

[25] R. E. Amaya, A. Momciu, and I. Haroun, "High-performance, compact quasi-elliptic band pass filters for V-band high data rate radios," *IEEE Trans. Components, Packag. Manuf. Technol.*, vol. 3, no. 3, pp. 411–416, Mar. 2013.

[26] Q.-Y. Guo, X. Y. Zhang, L. Gao, Y. C. Li, and J.-X. Chen, "Microwave and millimeter-wave LTCC filters using discriminating coupling for mode suppression," *IEEE Trans. Components, Packag. Manuf. Technol.*, vol. 6, no. 2, pp. 272–281, Feb. 2016.

[27] S. W. Wong, K. Wang, Z.-N. Chen, and Q.-X. Chu, "Electric coupling structure of substrate integrated waveguide (SIW) for the application of 140-GHz bandpass filter on LTCC," *IEEE Trans. Components, Packag. Manuf. Technol.*, vol. 4, no. 2, pp. 316–322, Feb. 2014.

[28] K. Wang, S.-W. Wong, G.-H. Sun, Z. N. Chen, L. Zhu and Q.-X. Chu, "Synthesis method for substrate-integrated waveguide bandpass filter with even-order Chebyshev response," *IEEE Trans. Components, Packag. Manuf. Technol.*, vol. 6, no. 1, pp. 126-135, Jan. 2016.

[29] Y. Li, L.-A. Yang, L. Du, K. Zhang, and Y. Hao, "Design of millimeter-wave resonant cavity and filter using 3-D substrate-integrated circular waveguide," *IEEE Microw. Wirel. Components Lett.*, vol. 27, no. 8, pp. 706–708, Aug. 2017.

[30] X. Shang, H. Yang, D. Glynn, and M. J. Lancaster, "Submillimeter-wave waveguide filters fabricated by SU-8 process and laser micromachining," *IET Microwaves, Antennas Propag. Spec.*, vol. 11, no. 14, pp. 2027–2034, Dec. 2017.

[31] O. Sushko, M. Pigeon, R. S. Donnan, T. Kreouzis, C. G. Parini and R. Dubrovka, "Comparative study of sub-THz FSS filters fabricated by inkjet printing, microprecision material printing, and photolithography," *IEEE Trans. on Terahertz Science and Technology*, vol. 7, no. 2, pp. 184-190, Mar. 2017.

[32] C. Arnold, J. Parlebas, and T. Zwickber, "Reconfigurable waveguide filter with variable bandwidth and center frequency," *IEEE Trans. Microw. Theory Tech.*, vol. 62, no. 8, pp. 1663–1670, Aug. 2014.

[33] D. Sun and J. Xu, "A novel iris waveguide bandpass filter using air gapped waveguide technology," *IEEE Microwave and Wireless Components Letters*, vol. 26, no. 7, pp. 475-477, Jul. 2016.

[34] W. J. Otter and S. Lucyszyn, "3-D printing of microwave components for 21st century applications," *IEEE MTT-S International Microwave Workshop Series on Advanced Materials and Processes for RF and THz Applications (IMWS-AMP)*, Chengdu, 2016, pp. 1-3.

[35] Z. Bing, Y.-X. Guo, H. Zirath, and Y. P. Zhang, "Investigation on 3-D-printing technologies for millimeter-wave and terahertz applications," *Proc. IEEE*, vol. 105, no. 4, pp. 723–736, Apr. 2017.

[36] M. D'Auria, W. J. Otter, J. Hazell, B. T. W. Gillatt, C. Long-Collins, N. M. Ridler, and S. Lucyszyn, "3-D printed metal-pipe rectangular waveguides," *IEEE Trans. Components, Packag. Manuf. Technol.*, vol. 5, no. 9, pp. 1339-1349, Sep. 2015.

[37] W. J. Otter, N. M. Ridler, H. Yasukochi, K. Soeda, K. Konishi, J. Yumoto, M. Kuwata-Gonokami and S. Lucyszyn, "3D printed 1.1 THz waveguides," IET Electronics Letters, vol. 53, no. 7, pp. 471-473, Mar. 2017.

[38] B. Zhang and H. Zirath, "Metallic 3-D printed rectangular waveguides for millimeter-wave applications," *IEEE Trans. Components, Packag. Manuf. Technol.*, vol. 6, no. 5, pp. 796-804, May 2016.

[39] W. J. Otter and S. Lucyszyn, "Hybrid 3-D-printing technology for tunable THz applications," *Proc. IEEE*, vol. 105, no. 4, pp. 756–767, Apr. 2017.

[40] A. Tamayo-Domínguez, J. Fernández-González and M. Sierra-Pérez, "Groove gap waveguide in 3-D printed technology for low loss, weight, and cost distribution networks," in *IEEE Transactions on Microwave Theory and Techniques*, vol. 65, no. 11, pp. 4138-4147, Nov. 2017.

[41] Ereš, Zoran; Vukomanović, Mladen; Šipuš, Zvonimir, "Gap waveguide leaky wave antenna realized in 3D printing technology," *22nd International Conference on Applied Electromagnetics and Communications (ICECom)*, Zagreb, 2016, pp. 1-4.

[42] J.-S. Hong and M. J. Lancaster, "Design of highly selective microstrip bandpass filters with a single pair of attenuation poles at finite frequencies," *IEEE Trans. Microw. Theory Tech.*, vol. 48, no. 7, pp. 1098–1107, Jul. 2000.

[43] H. Raza, J. Yang, P. Kildal and E. Alfonso, "Resemblance between gap waveguides and hollow waveguides," in *IET Microwaves, Antennas & Propagation*, vol. 7, no. 15, pp. 1221-1227, 10 December 2013.